Robust and Accurate Positioning Control of Solar Panel System Tracking based Sun Position Image

Lailis Syafa'ah
Electrical Engineering Department
University of Muhammadiyah Malang
Malang, Indonesia
lailis@umm.ac.id

Lailatul Fauziyah
Electrical Engineering Department
University of Muhammadiyah Malang
Malang, Indonesia
fauziyahlailatul17@gmail.com

Zulfatman Has
Electrical Engineering Department
University of Muhammadiyah Malang
Malang, Indonesia
zulfatman@umm.ac.id

Abstract—**This study contains the robust and accurate positioning control design for solar panel system consisting of elevation and azimuth axis tracker. The ultimate objective of the study is to ensure the solar panel move accurately to follow its tracking reference against mechanical load and other disturbances. The tracking reference was the images of actual sun position. Image processing result as the initial reference and high precision encoder as the controller feedback path were intended to obtain the accurate position of hardware response. Sliding Mode Controller (SMC) with Proportional Integral Derivative (PID) Sliding Surface was employed as control technique that guarantee the solar panel system robust against disturbances or load variation. The proposed method was evaluated through software simulation and hardware validation. The software for the simulation and validation was LabVIEW. While the software for image processing was Vision Assistant. From hardware validation, accuracy of the solar panel system to track the sun position image for elevation and azimuth were 2.622% (0.03007°) and 0.244% (0.00893°), respectively. These results indicate that the solar panel system was available to move accurately to track the sun position both in azimuth and elevation axis.**

Keywords— Solar tracker, position tracking, image processing, Sliding Mode Controller, PID sliding surface

I. INTRODUCTION

The most popular research topic on renewable energy is about solar energy that is focused on designing systems to optimize the efficiency of solar energy absorption. One interesting topic is a real time solar tracking system by facing the sun. Solar tracker can increase the output power up to 20-25% for single axis and 30-45% for dual axis. Azimuth & elevation solar tracking allows solar panel to be moved left to right direction by rotating the azimuth plane as well as upwards or downwards in the elevation plane [1, 2]. In this case the control systems is being very important to get the consistency of the system rotation. The precission solar tracking system will give higher efficiency, so the variational method has been applied to get more accurate tracking position. Such as uses the astronomical calculation, GPS, light sensors, until camera with image processing.

The image processing produces higher accuracy on the sun position detection, as known the error values result from the previous simulation study was 0.3688° (azimuth) and 0.3874° (elevation) [3]. In [4], the accuracy of tracking system without being affected by the weather can reach 0.1°. While in the other study [5] by designing system that was capable to detect sun position in cloudy weather can reach 0.04⁰. These advantages have been compared with the other research method, such as using astronomical calculations the error was 1.0997° (azimuth) and 1.2877° (elevation), LDR which can increase the error in precentages up to 18.13%, while using the photodiodes can reach until 5° error value [3,

6, 7]. These previous results shows that the image processing is capable to result very accurate object identification, because it can provide the sun centroid coordinate pixels precisely in real time. Greater resolution of the camera will provide better performance of solar tracking process [8]. The pixel position of the sun centroid is represented by x and y value which is represent the error value from the midpoint of camera frame. These values are used as the initial reference for azimuth and elevation axis to rotate.

The accuracy of the system won't be reached without the precission angle of servo motor rotation although the initial setpoint has very precission value. The servo motor in this system is an actuator that rotates to remove the sun position error. Servo motor is formed from DC motor which is controlled in closed loop system to rotate as much as the reference angle [9]. There are several servo controllers i.e. PID, Fuzzy Logic Controller, Neural Networks, and Line Quadratic-optimal Controller. But these controllers have less resistant to the external disturbance [10]. Moreover the DC motors have the nonlinearity, so the robust controller is needed. Sliding Mode Control (SMC) is one of the popular control strategies and powerfull control technology to deal with the nonlinearity. SMC has two main part, they are the *sliding function* and the *sliding surface*. Precise dynamic model are not required and the control algorithms can be easily implemented. However the parameters design of *sliding function* will affect the robustness of SMC [11].

In this study, Sliding Mode Controller with PID *sliding function* (SMC-PID) was applied to control the angular rotation of the DC motor. The SMC's *sliding surface function* parameters was design to optimized the control robustness. The initial reference is according to the image processing result, while the feedback signal is based on the encoder value. SMC is used to achieve the robustness to the system parameters variation and external disturbances. The main term is to get the most accurate and high precission panel position in order to track the sun position on azimuth and elevation angle.

II. SYSTEM MODELING

A. Sun Position Detection

Sun position detection consist of three steps, i.e. vision acquisition (capture the sun image with the camera from MyRIO), vision assistant (image processing), and the determination of the sun pixel position. Camera is used to take the sun picture that will be input for the image processing. The purpose of image processing is to determine the sun centroid location that will be represented in the cartesian coordinate of camera frame by the value of x and y.

The vision assistant program as the image processing which shown in Fig. 1, consist of 6 steps, ie. thresholding,

324

binary inversion, removing small objects, low pass filter, circle detection, and coordinate system determining.
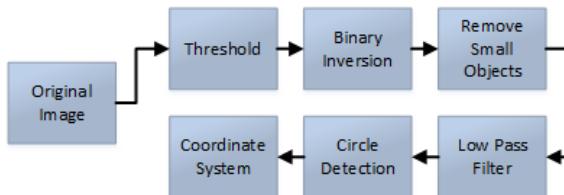

Fig. 1. Vision Assistant Block Program for Sun Detector

There are several image in Fig. 2 which shows the results of each image process sequence. Image (a) shows the original image of sun without cloud around it which will be processed by the vision assistant. Image (b) shows the threshold result which is consist of black and red color. Image (c) shows the binary inversion result which is the brighest area is the sun position area.

Fig. 2 (d) shows the advanced morphology result to remove small objects around the main circle. Image (e) shows the low pass filter result where the less obvious objects will be erased from the image. Then, the image (f) shows the circle detection result, in which we can see the position of the sun circle. The image is processed by coordinate system to obtain the coordinate point of the detected circle from the center frame.
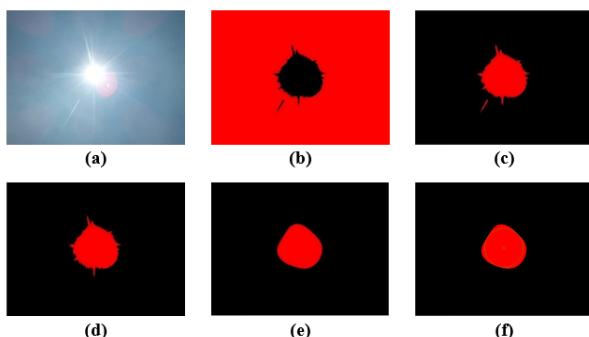
Fig. 2. Sun Detection Process of Vision Assistant

B. State Space Modeling

The DC motor modeling is a process to obtain mathematical model of the actuator. System identification procedures are performed with LabVIEW's existing features, Identification System in the Control and Simulation Toolkit [12].
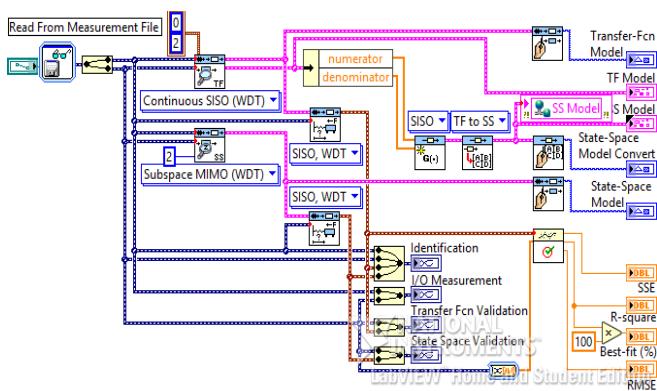
Fig. 3. LabVIEW Validation Program

By using validation process in Fig. 3, which was generated by parameter estimation, the elevation model can approach the real hardware with the percentage of best-fit up to 86.4%. The state equations of the elevation model as result in equations (1) and (2).

$$\frac{dx}{dt} = \begin{bmatrix} -0,618492 & -0,133284 \\ 0,125 & 0 \end{bmatrix} x(t) + \begin{bmatrix} 8 \\ 0 \end{bmatrix} u(t) \quad (1)$$

$$y(t) = [0 \quad 0,014768] \, x(t) + [0] \, u(t) \quad (2)$$

While the azimuth model results a better best-fit up to 97.2%, which indicates that the azimuth model has the higher fitness. Because there is no varied mechanical load which affects the system. The horizontal rotational has a stable load in almost all positions. The state equations of the azimuth model are expressed in equations (3) and (4) below.

$$\frac{dx}{dt} = \begin{bmatrix} -0,098421 & -0,051034 \\ 0,0625 & 0 \end{bmatrix} x(t) + \begin{bmatrix} 16 \\ 0 \end{bmatrix} u(t) \quad (3)$$

$$y(t) = [0 \quad 0,00313952] \, x(t) + [0] \, u(t) \quad (4)$$

C. PID Controller

PID controller has many advantages to system respons such as rise time, overshoot, and steady state. The formulation of PID controller is expressed in equation (5).

$$u(t) = K_p e(t) + K_i \int_0^t e(\tau) d\tau + K_d \frac{de(t)}{dt} \quad (5)$$

D. Sliding Mode Controller

The implementation of SMC based PID sliding surface will be modeled as following block diagram in Fig. 4.
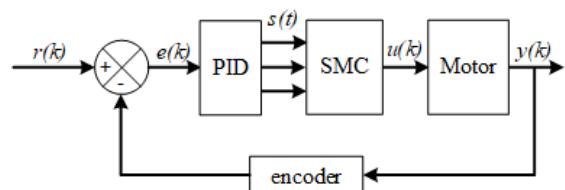
Fig. 4. Block Diagram of SMC-PID

The design is expected to reduce the effects of unwanted disturbances such as load and friction effects. After performing DC motor modeling, the PID will be added to minimize the rotational error between the motor output and reference value. The PID parameter tuning is done by manual tuning in the LabVIEW Control & Simulation toolkit. Then SMC will be applied to the system where the PID will be integrated as the sliding surface optimization of SMC controller intended for the chattering reduction. Basic principle of SMC with PID sliding surface can be seen in Fig. 5.

The kp, ki, and kd values are the PID parameters as the determinant of the SMC sliding surface value. The mathematical equation is as follows.

$$s(t) = k_p e(t) + k_i \int_0^t e(\tau) \, d\tau + k_d \dot{e}(t) \quad (6)$$

325
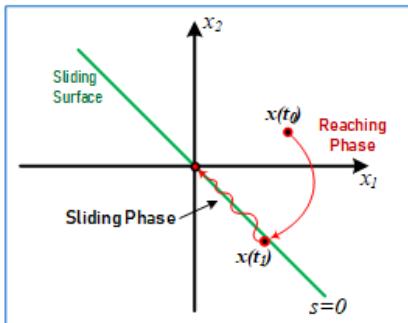
Fig. 5. The Response Illustration of SMC-PID

The first derivative of the sliding surface equation above is expressed in equation (7).

$$\dot{s}(t) = k_p \dot{e}(\mathrm{t}) + k_i e(t) + k_d \ddot{e}(t) \qquad (7)$$

The difference between the desired value with the actuator's actual position is formulated as the error value. The equation is expressed by equation (8).

$$e(t) = x_r(t) - x_p(t) \qquad (8)$$

The second derivative of the error equation above is expressed in the equation (9). This is coming from the second-order model obtained through from the DC motor identification.

$$\ddot{e}(t) = \ddot{x}_r(t) - \ddot{x}_p(t) \qquad (9)$$

The present value can be specified using the state space model parameters which is used. The second order of x_p is presented in equation (10).

$$\ddot{x}_p = -(A\dot{x} + Bx - Cu) \qquad (10)$$

The SMC control (u_SMC) consists of switching control (u_sw) and equivalent control (u_eq). The switching control is according to the reaching phase when s(t)≠0 while the equivalent control based on the sliding phase when s(t)=0. The general equation of SMC is denoted by equation (11).

$$u_{SMC}(t) = u_{sw}(t) + u_{eq}(t) \qquad (11)$$

The general switching control formula based on Lyapunov theorem [13] is shown in equation (12). This theorem has been used to reduce the chattering effect which belongs to the usual usw formulas.

$$u_{sw}(t) = tanh\left(\frac{s}{\varphi}\right) k_s \qquad (12)$$

The complete u_sw formula is expressed in equation (13) by substituting equation (6) to equation (12) above.

$$u_{sw} = tanh\left(\frac{k_p \mathrm{e}(t) + k_i \int_0^t e(\tau)\, d\tau + k_d \dot{e}(t)}{\varphi}\right) k_s \qquad (13)$$

Then the equivalent control can be obtained from the derivative of the sliding surface equation. This is obtained by substituting equation (9) and (10) to equation (7). The result is denoted in equation (14).

$$\dot{s}(t) = k_p \dot{e}(\mathrm{t}) + k_i e(t) + k_d \{\ddot{x}_r + A\dot{x} + Bx - Cu\} \qquad (14)$$

When s=s(t)=0, the sliding control will be executed because the sliding value has been reached. The equivalent control of SMC can be formed from equation (14) by assume the s(t)=0 that is represented in equation (15).

$$u_{eq} = \frac{(k_p \dot{e}(\mathrm{t}) + k_i e(t) + k_d \{\ddot{x}_r + A\dot{x} + Bx\})}{k_d Cu} \qquad (15)$$

Those formulas were applied to the LabVIEW which is shown in Fig. 6 below.
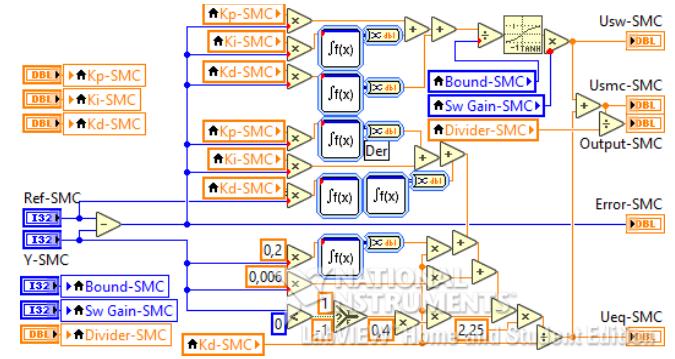
Fig. 6. LabVIEW Program of SMC-PID Controller

E. Simulation and Hardware Verification

General block diagram of the solar tracking system and the proposed control scheme can be seen in Fig. 7. below. It shows how the overall system works from input (image) to output (elevation and azimuth position).
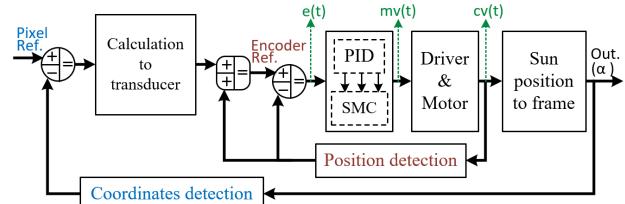
Fig. 7. Block Diagram of The Overall System

The hardware validation process is performed to ensure the simulated SMC-PID design can be applied actually. However, simulation also need to be done before the hardware validation to ensure the proposed algorithms are properly constructed and determine the controller parameters which is implemeted to the hardware. The elevation and azimuth position experimental validations are performed separately, using the PID and SMC-PID controllers. Due to the simulation results several parameters value with the best response are obtained and prepared for the hardware validation. Table I and Table II represent the control parameters of PID and SMC controllers, respectively.

TABLE I. PARAMETERS VALUE OF PID GAIN

Parameter	Elevation	Azimuth
Kp	750	1000
Ki	0	0
Kd	350	3700

TABLE II.   PARAMETERS VALUE OF SMC-PID GAIN

Parameter	Elevation	Azimuth
Kp	4000	40000
Ki	0	0
Kd	1000	20000
Boundary	15	15
Divider	5	1
Switching gain	10000	500

The hardware used due for the experimental validation is shown in Fig. 8. The main components of the hardware consists of camera, servo motors, encoders, power supply, and electrical module.
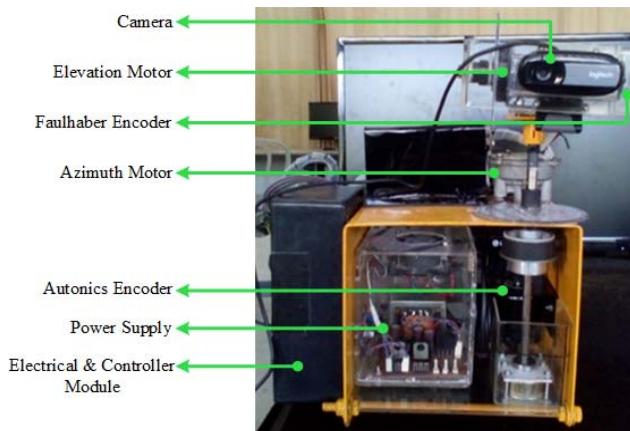

Fig. 8.   Prototype of The Elevation and Azimuth Tracker

III.   RESULTS AND DISCUSSION

A.   Encoder Evaluation

From the test, the elevation angle 180˚ and the azimuth angle 360˚ of the prototype were obtained as depicted in Fig. 9 and Fig. 10 below.

Fig. 9.   Elevation Angle 180˚

Fig. 10. Azimuth Angle 360˚

From these results we can obtain the actuator ratio. The elevation actuator rotated 180˚ when the incremental of faulhaber encoder reached 1272. While the azimuth actuator rotated 360˚ when the incremental of autonics encoder reached 10840. From those experiments, the encoder and angle ratio of the elevation and azimuth can be formulated with the equation (16) and equation (17), respectively.

$$\frac{elevation\ angle}{elevation\ encoder} = \frac{180^0}{1272} = \frac{1^0}{7,067} = \frac{0,1415^0}{1} \quad (16)$$

$$\frac{azimuth\ angle}{azimuth\ encoder} = \frac{360^0}{10840} = \frac{1^0}{30,111} = \frac{0,0332^0}{1} \quad (17)$$

B.   Sun Position Conversion

Object tracking process was done to obtain the comparison between the pixel values camera to encoder. The object being tracked was the LED (Light Emitting Diode) instead of the actual sun for laboratory scale testing. From the experiment, the error pixel for the initial LED position was 238 (for x value) and 315 (for y value), the hardware should be rotated until the LED reaches the midpoint of the camera frame. To reaches the (0,0) pixel position coordinates the azimuth encoder changed as much as 121 points, while the elevation 54 points. So the pixel to encoder ratio of both axes can be calculated as the equations (18) and (19).

$$\frac{y\ value}{elevation\ encoder} = \frac{315}{54} = \frac{1}{0,1714} = \frac{5,8333}{1} \quad (18)$$

$$\frac{x\ value}{azimuth\ encoder} = \frac{238}{121} = \frac{1}{0,5084} = \frac{1,9669}{1} \quad (19)$$

C.   Hardware Validation

Validation of the proposed PID and SMC-PID controllers were confirmed through experiments on the hardware. The experiments were performed for the elevation and azimuth axis separately.

The SMC-PID and PID implementation was done directly to the hardware. The random setpoint signal value was given to analyze the system response in the CW or CCW direction.
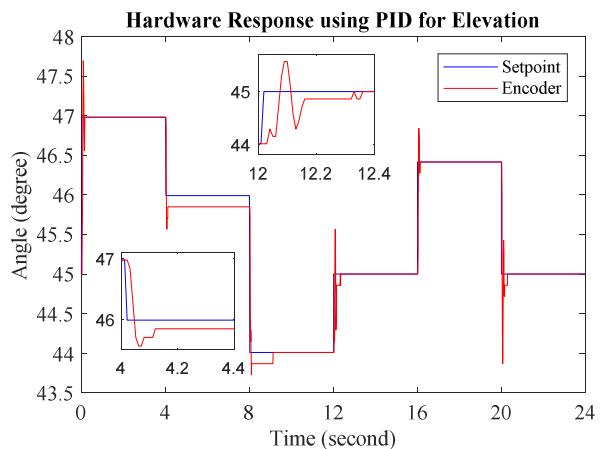

Fig. 11. Elevation Hardware Response with PID Controller

327

As can be seen in Fig. 11, in the 4th second the encoder (position) response with PID cannot reach the setpoint (reference). But, it still can reach the setpoint at the rest of the time with spike in several moments. This deficiency occurs due to PID's inability to withstand the mechanical load beyond the limits.

Hardware Response using SMC-PID for Elevation
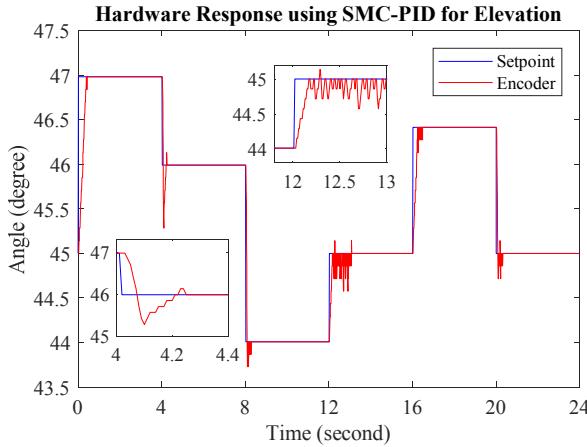
Fig. 12. Elevation Hardware Response with SMC-PID Controller

However, as shown in Fig. 12, the output position of the hardware available to reach the reference in the whole of time without any spikes. The response also maintain in stable in the reference. However, due to drawback of SMC, chattering was exist in certain parts of output response. A higher chattering indicates that the SMC receive a high disturbance. The highest overshoot was at the 4th second, but it wasn't as high as PID's overshoot with the error 5 encoder values.

The azimuth axis response with PID and SMC-PID controllers, respectively are shown in Fig. 13 and Fig. 14 below.

Hardware Response using PID for Azimuth
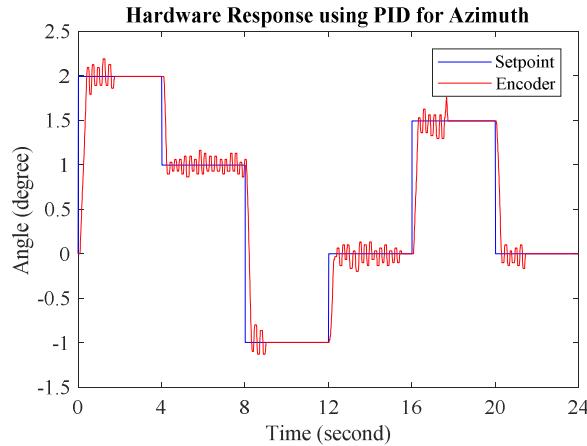
Fig. 13. Azimuth Hardware Response with PID Controller

The output response of the system with PID controller as depicted in Fig. 13, it can be seen that response was capable to reach the reference, but with several oscillations exist in the change of reference. The oscillation was caused by the readability of azimuth sensor was very high. Such that, the small motor rotation which crosses the setpoint (overshoot) reversed the error and caused the oscillation.

While Fig. 14 shows that the output response of the azimuth system with SMC-PID controller can reach the

reference faster than the PID controller. It was due to a high switching gain of the SMC that was capable to increase the system's power to move the hardware faster. However, the SMC switching gain effect occurred continously, even though it did not out of the reference value. Meanwhile if the switching gain was minimized, it reduced the oscillation, but with a longer rise time. Therefore a manual setting on the switching gain becomes an important point to do.

Hardware Response using SMC-PID for Azimuth
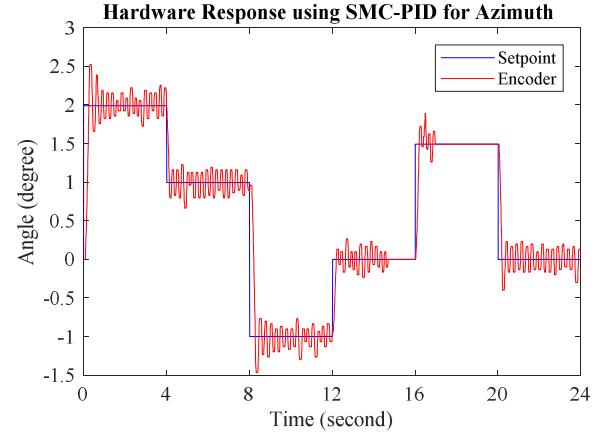
Fig. 14. Azimuth Hardware Response with SMC-PID Controller

D. Validation Accuracy

This test was performed to obtain the error value of azimuth and elevation tracking system designed. The position error of the sun image is described in pixels. Then from the pixel error the position error can be calculated using equations (18) to (19) to find out how much the error angle and encoder value that must be driven by the actuator to eliminate all the errors.

(a)   **(b)**   **(c)**

(d)   **(e)**   **(f)**
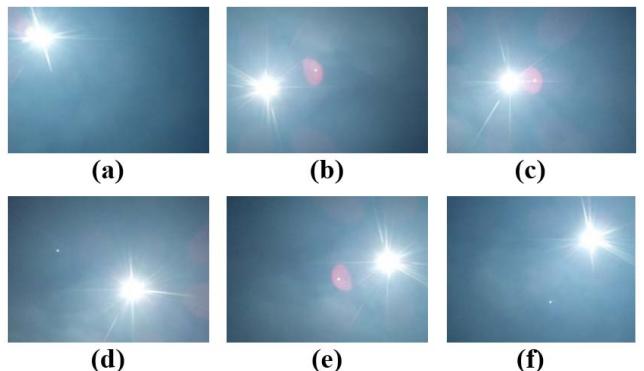
Fig. 15. Varied Sun Position Image

Fig. 15 shows some photos of various sun positions to be tested. Every image has error in elevation and azimuth axis. Each of them has the angle and encoder errors conversion from the detected pixel values. The calculation of encoders (calc.) must be close to the integer values (act.), because the sensor output wass read as an integer. The hardware validation process was done by giving the encoder setpoints to the both axis separately.

$$Angle\ Error = |\ Act.Angle - Calc.Angle\ | \qquad (20)$$

The Angle Error calculation above is needed to get the error values between the Calculation and Actual Angle. This error was inflicted by the rounding of encoder calculation

328

(the original conversion results from the pixel error) results to get the actual encoder as the integer values. Then the following graphs show the results of the hardware response with the converted amplitude in angle units.

While in order to calculate the accuracy of position control results that are implemented to the hardware. The average of each error values on both axis (elevation & azimuth) can be calculated by equation below.

$$Average\ Error = \left(\sum_{i=1}^{n} Angle\ Error\ (n)\right)/n \qquad (21)$$

The hardware validation results summary can be seen in Table III and Table IV below which shows the elevation and azimuth results, respectively.

TABLE III. VALIDATION RESULT OF ELEVATION (Y)

Image	Pixel	Calc. Angle	Act. Angle	Error (degree)	Error (%)
(a)	211	5,22524˚	5,23585˚	0,01061˚	0,203
(b)	-32	-0,79245˚	-0,84906˚	0,05660˚	7,142
(c)	-18	-0,44575˚	-0,42453˚	0,02123˚	4,763
(d)	-117	-2,89741˚	-2,83019˚	0,06722˚	2,320
(e)	34	0,84198˚	0,84906˚	0,00708˚	0,841
(f)	155	3,83844˚	3,82075˚	0,01769˚	0,461
Average Error				0,03007˚	2,622

TABLE IV. VALIDATION RESULT OF AZIMUTH (X)

Image	Pixel	Calc. Angle	Act. Angle	Error (degree)	Error (%)
(a)	-337	-5,68999˚	-5,67897˚	0,01102˚	0,194
(b)	-317	-5,35231˚	-5,34686˚	0,00544˚	0,102
(c)	-127	-2,14430˚	-2,15867˚	0,01437˚	0,670
(d)	126	2,12741˚	2,12546˚	0,00195˚	0,092
(e)	315	5,31854˚	5,31365˚	0,00488˚	0,092
(f)	300	5,06527˚	5,08118˚	0,01591˚	0,314
Average Error				0,00893˚	0,244

Analysis of the system accuracy from the data specified in the above table has been done successfully. It can be seen at a glance that most of the azimuth Angle Error are less than the elevation. It can be confirmed by the Average Error rows that shows the azimuth error value is 0,244% with the angle accuracy 0,00893˚ while the elevation is 2,622% with the angle accuracy 0,03007˚. So we can conclude the angle tracking ability of azimuth axis is more accurate than elevation.

IV. CONCLUSION

The method applied by using SMC-PID controller can provide the ability of the system to track the sun position image accurately. A more accurate sensor on the azimuth axis causes the angular tracking accuracy is higher. While the mechanical load on the elevation axis can be covered by the controller. This final project results can prove that with the SMC-PID controller, the elevation system can withstand the mechanical load variations in the elevation angle. While for the addition of position sensor (encoder) with high accuracy, the azimuth system can obtain the most high tracking accuracy. The accuracy of solar tracking system is expected to optimize the performance of solar panels without being affected by the mechanical load on the actual system.

REFERENCES

[1] V. Bosetti, "The Future Prospect of PV and CSP Solar Technologies: An Expert Elicitation Survey," *Energy Policy 49,* pp. 308-317, 2012.

[2] G. J. Prinsloo, Automatic Positioner and Control System for A Motorized Parabolic Solar Reflector, Maitland-South Africa: Stellenbosch University, 2014.

[3] M. Mirdanies and R. P. Sapura, "Dual-axis Solar Tracking System," in *International Conference on Sustainable Energy Engineering and Application (ICSEEA)*, Indonesian Institute of Sciences (LIPI), 2016.

[4] M. M. Arturo and G. P. Alejandro, "High-Precision Solar Tracking System," *World Congress on Engineering,* vol. II, 2010.

[5] C. D. Lee, H. C. Huang and H. Y. Yeh, "The Development of Sun-Tracking System Using Image," *Journal of Sensors,* vol. 13, pp. 5448-5459, 2013.

[6] A. Zakariah, J. J. Jamian and M. A. Yunus, "Dual-Axis Solar Tracking System Based on Fuzzy Logic Control and Light Dependent Resistors as Feedback Path Elements," *IEEE (SCOReD),* pp. 139-144, 2015.

[7] M. Haryanti, A. Halim and A. Yusuf, "Development of Two Axis Solar Tracking Using Five Photodiodes," *IEEE (EECCIS),* pp. 40-44, 2014.

[8] H. A. Sohag, M. Hasan, M. Khatun and M. Ahmad, "An Accurate and Efficient Solar Tracking System Using Image Processing and LDR Sensor," *IEEE (EICT),* pp. 522-527, 2015.

[9] G. A. Zarkar and S. S. Sankeshwari, "Simulation of DC Servo Motor Position Control using Sliding Mode Technique," *International Journal of Advances in Engineering & Technology (IJAET),* vol. 7, no. 6, pp. 1882-1888, 2015.

[10] C. Vivekanandan, R. Prabhakar and D. Prema, "Stability Analysis of a Class of Nonlinear Systems Using Discrete Variable Structures and Sliding Mode Control," *International Journal of Electrical and Computer Engineering,* vol. 2, no. 5, pp. 856-862, 2008.

[11] T. Chamsai, P. Jirawattana and T. Radpukdee, "Sliding Mode Control with PID Tuning Technique: An Application to a DC Servo Motor Position Tracking Control," *Energy Research Journal,* vol. 1, no. 2, pp. 55-61, 2010.

[12] M. P. Badramurti, E. A. Hakim and N. A. Mardiyah, "Analisis dan Desain Kontroler Fuzzy-PID pada Plant Motor DC Berbasis Spreadsheet menggunakan Pendekatan Metode Numerik," Muhammadiyah Malang University, Malang, 2017.

[13] C. C. Soon, R. Ghazali, H. I. Jaafar, S. Y. S. Hussien, S. M. Rozali and M. Z. A. Rashid, "Optimization of Sliding Mode Control using Particle Swarm Algorithm for an Electro-hydraulic Actuator System," *Journal of Telecommunication, Electronic and Computer Engineering,* vol. 8, no. 7, pp. 71-76, 2016.